MSDE

MINI REVIEW

View Article Online
View Journal | View Issue

Cite this: *Mol. Syst. Des. Eng.*, 2019, 4, 566

Photonic nanoarchitectonics with stimuli-responsive 2D materials

Pirmin Ganter[a] and Bettina V. Lotsch *[abc]

Received 15th December 2018,
Accepted 6th March 2019

DOI: 10.1039/c8me00112j

rsc.li/molecular-engineering

The ability to produce structural color from inherently colorless materials, similar to that in butterfly wings and beetle shells, has attracted considerable research interest over the last three decades. Despite their extraordinary properties and performances, the field of structural colors based on inherently functional 2D materials only took off recently. In this minireview, we highlight the diversity of 2D materials utilized for achieving structural coloration in different architectures. We summarize the large tunability of photonic architectures based on 2D materials and emphasize their extraordinary dynamic response induced by external stimuli. Subsequently, recent strategies to tailor their properties with molecular and structural approaches are discussed. Finally, we point out promising future directions in this emerging field.

Design, System, Application

As 2D materials are coming of age, their richness in composition, structure and properties offer a unique platform for the design of tailor-made nanoscale building blocks for functional devices. Combining the chemical scope, diverse optical properties and stimuli-responsive nature of 2D materials and their ensembles with the recent advancement in liquid-assisted assembly strategies, 2D materials have emerged as versatile building blocks in thin film-based photonic architectures, including Fabry–Pérot interference filters and 1D photonic crystals. To impart such architectures with maximum functionality, design strategies range from molecular level approaches such as ion exchange and intercalation, to morphology engineering such as porosity tuning. The integration of 2D materials into photonic architectures has opened up new horizons in the realization of smart devices, ranging from vapor and pressure sensors to functional surfaces allowing for the touchless tracking of finger motions. On a more fundamental level, thin films exhibiting tunable structural color allow for the observation of otherwise optically silent processes with the naked eye, such as intercalation into 2D materials. Cast into photonic architectures, the unique versatility of 2D materials and their molecularly engineered counterparts can be harvested to push the limits of label-free sensing, anti-counterfeiting, radiation shielding, photovoltaics, display technology, and beyond.

Structural color – overview and concepts

Iridescent soap bubbles, opals, beetle shells and butterfly wings are naturally occurring nanostructures that fascinate due to their ability of producing a wide range of colors from inherently colorless materials (Fig. 1a–c).[1–4] Over the last three decades, substantial progress has been achieved in creating such structural colors in the laboratory.[5–15] As opposed to the colors of dyes and pigments, which are based on the absorption of light, structural color arises due to diffraction, refraction and reflection of light by submicron scale structures.[1,7,8,10] The various artificial architectures that produce structural colors in the laboratory range from simple thin films to more complex 1D, 2D and 3D periodic assemblies of dielectric materials, termed photonic crystals (PC) Fig. 1d.[8,10] A major driving force accelerating the fabrication of complex photonic architectures has been the rapid development of assembly strategies for nanomaterials that exploit and maximize novel functionalities originating from mutual interactions between the individual building blocks.[16–19] Such emerging functionalities in hierarchically organized nanostructures can be considered a hallmark of the design principle known as nanoarchitectonics.[16,17]

The origin of the displayed structural color of the simplest photonic architectures like thin films and one-dimensional photonic crystals (1D PCs), can be derived from the condition for constructive interference by a combination of the Bragg and Snell laws (see Fig. 1e):[11,15,20]

$$m\lambda = 2l\sqrt{{n_{\mathrm{eff}}}^2 - \sin^2(\theta)} \quad (1)$$

Hereby, m is an integer value, λ is the wavelength for which constructive interference occurs, n_{eff} is the effective refractive index (RI) of the layer (in Fabry–Pérot sensors) or bilayer (in case of a 1D PC; $n_{\mathrm{eff}} = (n_1l_1 + n_2l_2)/(l_1 + l_2)$, with l_1 +

[a] Max Planck Institute for Solid State Research, Heisenbergstrasse 1, 70569 Stuttgart, Germany. E-mail: b.lotsch@fkf.mpg.de
[b] Department of Chemistry, Ludwig-Maximilians-Universität (LMU) München, Butenandtstrasse 5-13, 81377 Munich, Germany
[c] Nanosystems Initiative Munich (NIM) and Center for Nanoscience, Schellingstraße 4, 80799 Munich, Germany

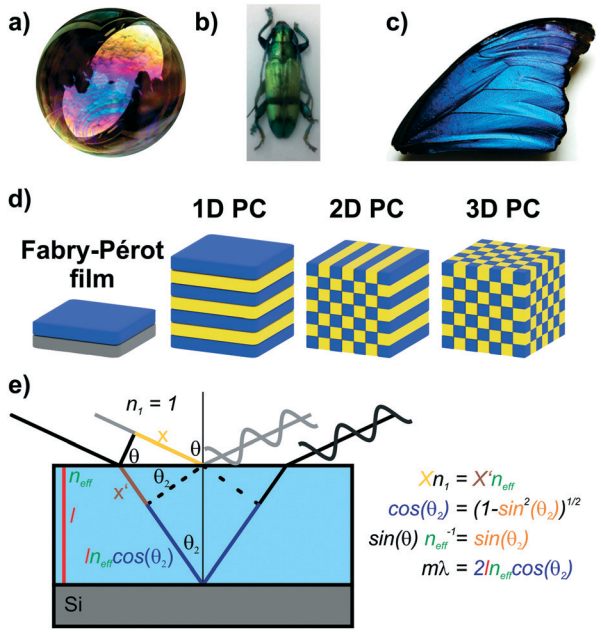

Fig. 1 Structural color in nature and everyday life serve as inspiration for artificial photonic architectures: a) interference color of a soap bubble, b) *Tmesisternus isabellae* beetle shell showing structural color,[2] c) *Morpho* butterfly wing.[1] d) Common photonic architectures realized in the laboratory to achieve structural coloration.[21] From left to right: thin film on silicon substrate, 1D PC, 2D PC and 3D PC. e) Visualization of Bragg–Snell law. Panel a) reprinted and adapted with permission from Wikimedia Commons, Copyright 2007 Brocken Inaglory. Panel b) reprinted with permission from ref. 2, Copyright 2017 Springer Nature. Panel c) Reprinted with permission from ref. 1, copyright 2018 American Chemical Society.

$l_2 = l$),[12] and θ the illumination angle. Under normal incidence, this equation transforms to:

$$m\lambda = 2n_{\text{eff}}l \tag{2}$$

for a thin film,[22–24] and

$$m\lambda = 2\,(n_1l_1 + n_2l_2) \tag{3}$$

for a 1D PC.[9,12] For the latter, l_1 and l_2 are the layer thicknesses and n_1 and n_2 are the RIs of the individual layers contributing to the bilayer. The condition of constructive interference leading to maximum reflectance in a 1D PC is equivalent to the photonic stop band or photonic band gap. From eqn (2) and (3), one can see that by changing the material thickness or the RI, a color change can be achieved. Hence, stimuli which induce a change in either n_i, or l_i, or both, can be detected (Fig. 2).[9,10,12,14,25]

The first generation of stimuli-responsive 1D PC was based on changes in the RI of porous nanoparticles.[9,26–29] Although some progress regarding selectivity could be achieved through functionalization[27,30,31] and use of inherently functional MOFs[32,33] or zeolite NPs,[34] a major drawback remained: the intrinsically limited sensitivity due to small RI changes in the layers (typical solids and liquids have refractive indices between 1 and 3, with most solvents having RIs around 1.3–1.5). This low sensitivity could be circumvented in the second generation of 1D PCs by utilizing swellable polymers as their active component.[35–39] The polymer-based 1D PC show higher sensitivities as they are operated on layer thickness change; however, they exhibit rather long response times on the order of several seconds up to minutes and, being soft materials, have intrinsic stability issues, for example, to mechanical deformation, temperature and chemicals. Therefore, the search for stable stimuli responsive materials for 1D PCs, operating based on fast and reversible layer thickness changes, led to the third generation of 1D PCs based on inorganic 2D materials (nanosheets).[40,41] The advantages for creating structural colors based on 2D materials include their tunable 2D morphology, inherent responsiveness to stimuli by swelling, diversity in composition and structure, and existence of methods to tailor and fine-tune their properties.[42–49]

Pirmin Ganter

Pirmin Ganter obtained his PhD degree under the supervision of Bettina V. Lotsch from the University of Munich (LMU Munich) in 2018. He is currently working as a scientist in the Lotsch group at the Max Planck Institute for Solid State Research. His research interests include the synthesis, assembly and functionalization of 2D materials for various applications.

Bettina V. Lotsch

Bettina V. Lotsch received her Ph.D. from LMU Munich in 2006. After a postdoctoral stay at the University of Toronto she was appointed associate professor at LMU Munich. Since 2017 she has been Director at the Max Planck Institute for Solid State Research in Stuttgart. Her research interests are at the interface between solid-state chemistry, nanochemistry, and molecular chemistry and include porous frameworks and 2D materials for sensing and energy conversion. Bettina was named Fellow of the Royal Society of Chemistry in 2014 and is recipient of an ERC Starting grant (2014) and the EU-40 Materials Prize 2017 from the European Materials Research Society (EMRS).

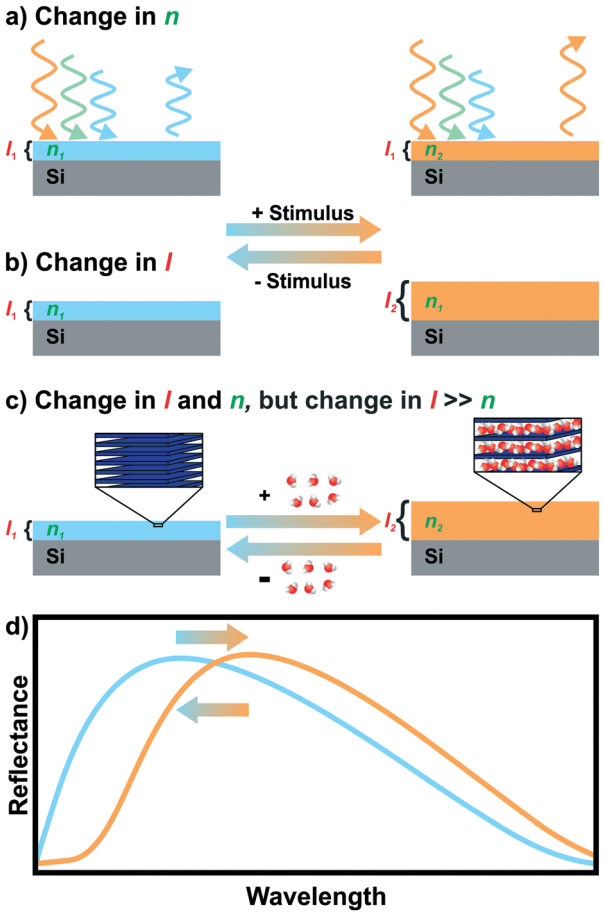

Fig. 2 Stimulus sensing with a photonic thin film. A change caused by a stimulus in the refractive index a), or layer thickness b), or both c), can result in a change of the displayed structural color d). In the case of c), which is the default situation in nanosheet-based thin films, the change in the layer thickness is much more pronounced compared to the decrease of the refractive index. Therefore, an overall redshift in the reflectance spectrum is observed, d).

However, they remained almost unexplored until recent times due to the limited availability of nanosheets and efficient processing techniques for 2D materials, despite early efforts with 2D materials in thin film interference sensors.[50] With the recent advances in nanosheet processing protocols and tailoring methods,[43,51–54] 2D materials made their way into the field of structural colors.[41,55–59]

Although there are excellent recent reviews on structural colors and their applications,[7,8,10–12] 2D materials appear only as minor points in these reviews as most of the research in this field is still carried out with nanoparticles and polymers despite considerable drawbacks compared to 2D materials.

With this review, we thus shine a light on photonic nanostructures based on 2D materials in order to reveal their potential as colorimetric sensors. We first give an overview of the tunable structural colors realized with a large variety of 2D materials. As nearly all of the 2D material based structures are able to change their thickness by swelling, we highlight recent examples of stimuli responsive behaviour enabling the tracking of otherwise optically silent processes. This is followed by strategies to tailor their swelling behaviour leading to rationally designed sensors and micron scale patterns of nanosheets. In the last section, promising future directions are presented for structural colors based on such 2D materials. With this review we thus illustrate the enormous potential of 2D materials as tailorable building blocks for nanostructured color sensors and beyond.

2D materials for structural coloration

Large quantities of 2D materials can be derived from solvent-based delamination of layered materials,[43,60,61] of which the most efficient routes are liquid-phase, redox-mediated and ion exchange exfoliation.[42–44,51,60,62,63] Details on these methods have been covered in recent review articles.[43–45,51] A wide variety of nanosheets with diverse composition and properties has been obtained by these exfoliation methods.[42,44,45,62] Right after exfoliation some nanosheets can form liquid crystals which coherently scatter light, leading to structural colors (see Fig. 3a).[64,65] However, to make more efficient use of the structural color for sensing, the nanosheets need to be assembled into solvent-free photonic architectures.[40,50,66,67] To achieve this, the most important, liquid-assisted strategies for nanosheets are spin or dip-coating.[27,40,41,50,56,58,68–70] The crucial parameters for nanosheet deposition using these methods are the concentration, wetting properties and volatility of the solvent.[40,41,56,68] The thickness of the nanosheet layer can be altered by adjusting the spin-coating speed, concentration of the nanosheets, or by repeating the deposition procedure.[41,55,59,68] This control of the layer thickness allows to adjust the structural color throughout the visible spectral range (Fig. 3b–f).[40,41,55,56,59]

Until now, a wide variety of nanosheets has been utilized to achieve structural color, as summarized in Fig. 3 and Table 1.[40,41,55–59,65,67,71,72] However, an even larger, rapidly growing library of 2D materials exists, which holds promise for a yet more diverse and powerful set of sensing properties that can be harnessed in the future.[42,44,73–78] The variety of nanosheets used for achieving structural colors range from antimony phosphates,[41,56,72] layered double hydroxides[59,79] to layered silicates such as clays,[40,50,66,80] and the architectures include thin films, 1D and 3D PCs, besides liquid crystals (Fig. 3, Table 1). Taking a closer look at the optical properties of 2D materials, one can see that low to medium RI materials (Mg–Al–NO_3 LDH, $H_3Sb_3P_2O_{14}$, $H_{1-x}TBA_xTaP_2O_8$, LAPONITE®)[41,50,56] and high RI materials (*e.g.* lithium tin sulfide (LTS) or $HCa_2Nb_3O_{10}$)[55,57,81] are available alike, allowing for a large optical contrast with other materials in 1D, 2D and 3D PCs (Table 2). The precise control of the stop band position can be utilized in wavelength selective mirrors, *e.g.* dichroic mirrors, which find applications in photovoltaics, for instance in perovskite and dye sensitized solar cells, in lasers, in bank note security

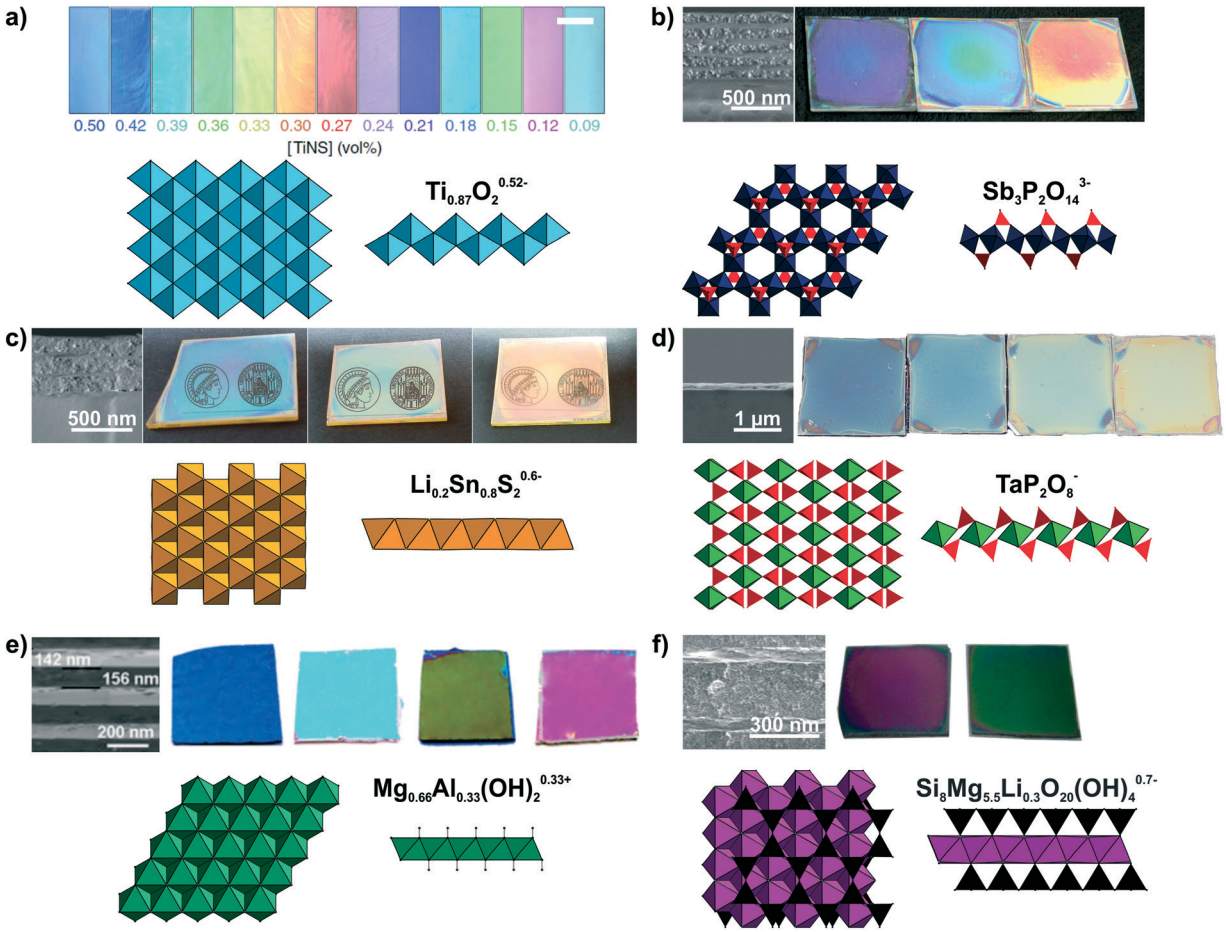

Fig. 3 Modulation of structural colors from 2D materials. For all panels a formula of the nanosheet composition and top and side view of the respective nanosheet structure is shown. The TiO_6 octahedra are light blue, SbO_6 octrahedra dark blue, PO_4 tetrahedra red, $Li_{0.2}Sn_{0.8}S_2$ octahedra orange, TaO_6 octahedra green, $Mg_{1-x}Al_xO_6$ octahedra dark green, SiO_4 tetrahedra black and $(Mg_xLi_y)O_4F_2$ octahedra purple. The tunable structural colors result from variations in the spin-coating speed or repetition except of a). a) Lepidocrocite-type $Ti_{0.87}O_2^{0.52-}$ forming a highly oriented liquid crystal in the presence of a magnetic field. Depending on the nanosheet concentration, the interlayer spacing changes and hence, the structural color.[65] b) $H_3Sb_3P_2O_{14}/SiO_2$ 1D PCs with different nanosheet layer thicknesses including a SEM cross-section image to highlight the morphology difference of the nanoparticle (NP) and nanosheet layer.[41] c) Lithium tin sulfide (LTS) 1D PCs with different nanosheet layer thicknesses. As seen in the SEM cross-section compared to $H_3Sb_3P_2O_{14}/SiO_2$ 1D PCs a lower number of total layers is sufficient for achieving a high reflectance due to the higher refractive index contrast in the LTS/SiO_2 1D PCs.[55] d) SEM cross-section of a $H_{1-x}TBA_xTaP_2O_8$ thin film on a silicon substrate and images of films with different thicknesses.[56] e) Mg–Al–NO_3 LDH/TiO_2 1D PCs with adjustable structural colors.[59] f) LAPONITE®/TiO_2 1D PCs with different layers thickness and representative SEM cross-section image of the sample. As a structural model a closely related hectorite layer is depicted instead of LAPONITE®.[40] Panel a) reprinted and adapted with permission from ref. 65, Copyright 2016 Springer Nature. Panel b) reprinted and adapted with permission from ref. 41, Copyright 2015 John Wiley and Sons. Panel c) reprinted and adapted with permission from ref. 55, Copyright 2018 John Wiley and Sons. Panel d) reprinted and adapted with permission from ref. 56, Copyright 2017 John Wiley and Sons. Panel e) reprinted and adapted with permission from ref. 59, Copyright 2012 the Royal Society of Chemistry. Panel f) reprinted and adapted with permission from ref. 40, Copyright 2008 John Wiley and Sons.

features or for the colourful design of buildings with radiation shielding properties.[8,11–13]

Stimuli induced color changes based on 2D material structures

Besides making use of the "static" structural color of photonic structures, applications relying on dynamic color changes triggered by external stimuli are heavily investigated.[7,11] The main utilization of dynamic structural color changes is in the field of sensing.[7,10,11,25] Sensors based on structural colors can offer significant advantages compared to other sensor systems: They are label free sensors requiring no external power supply, offer a simple optical readout and are small, portable and inexpensive.[10,25]

Current challenges in the field of photonic sensors include the design of sensors with better selectivity, sensitivity, speed, stability and alternative readout schemes.[10,25] Due to their fast swelling behaviour and tunability, 2D materials show great potential for improving these characteristics of photonic sensors.[46,47,49,88–91]

Table 1 Overview of photonic architectures showing structural coloration based on 2D materials. Details are given on the type of architectures, their composition, respective role of the nanosheet component and main applications

Composition (Nanosheet)	Type of architecture	Role of nanosheet	Main points
LAPONITE®/PDDA (ref. 50)	Thin film	Stimuli responsive, swelling	Humidity sensing
LAPONITE® ($Na_{0.7}[(Si_8Mg_{5.5}Li_{0.3})O_{20}(OH)_4]$) (ref. 40)	Thin film	Stimuli responsive, swelling	Surfactant detection and concentration determination based on ion exchange
LAPONITE®/SiO_2 (ref. 40)	1D PC	Stimuli responsive, swelling	Uptake and release kinetics of surfactants & cyclability (mainly ion exchange)
LAPONITE®/TiO_2 (ref. 40)			
LAPONITE® (ref. 80)	Thin film	Stimuli responsive, swelling	Uptake and release kinetics of surfactants & cyclability (mainly ion exchange)
Porous LAPONITE®/TiO_2 (ref. 80)	1D PC and		
TiO_2/SiO_2 with defect LAPONITE® (ref. 80)	Defect 1D PC	Stimuli responsive, swelling	
Porous LAPONITE®/LAPONITE® (ref. 66)	1D PC	Stimuli responsive, swelling	Porous LAPONITE® layers by templating
Porous LAPONITE® (ref. 66)	3D PC	Stimuli responsive, swelling	Porous LAPONITE® layers by templating
Mg–Al–NO_3 LDH/TiO_2 (ref. 59)	1D PC	Stimuli responsive, refractive index change by phase transition	Temperature sensing
MMO (derived from Mg–Al–NO_3 LDH)/TiO_2 (ref. 79)	1D PC	Converted into MMO[a]	Sensing of vapors & humidity based on refractive index changes of MMO[a]
$H_{0.52-x}TMA_xTi_{0.87}O_2$ (lepidocrocite-type) (ref. 65)	Liquid crystal	Stimuli responsive, swelling	Sensing of pH, temperature and magnetic field orientation
Silk/silk-TiO_x (ref. 71)	1D PC	Provide refractive index contrast, stimuli responsive, swelling and refractive index change	Humidity sensing
$H_3Sb_3P_2O_{14}$/SiO_2 (ref. 41)	1D PC	Stimuli responsive, swelling	Humidity sensing, touchless positioning interface, transparency switching
$H_3Sb_3P_2O_{14}$/TiO_2 (ref. 41)	1D PC	Stimuli responsive, swelling	Humidity sensing, touchless positioning interface
$HSbP_2O_8$/TiO_2 (ref. 72)	1D PC	Stimuli responsive, swelling	Humidity and vapor sensing
$H_{3-x}TBA_xSb_3P_2O_{14}$ (ref. 56)	Thin film	Stimuli responsive, swelling, host for ion exchange	Impact of interlayer cation on humidity and vapor sensing characteristics
$H_3Sb_3P_2O_{14}$ (ref. 56)	Thin film		
$H_{1-x}TBA_xTaP_2O_8$ (ref. 56)	Thin film		
$H_{1-x}TBP_xTaP_2O_8$ (ref. 56)	Thin film		
$H_3Sb_3P_2O_{14}$ with amines (ref. 82)	Thin film	Stimuli responsive, swelling, host for intercalation of primary and tertiary alkylamines	Differentiation of primary and tertiary alkylamines, area resolved intercalation, utilization of amine functionalization for vapor sensing
$H_3Sb_3P_2O_{14}$/TiO_2 with amines (ref. 83)	1D PC	Stimuli responsive, swelling, host for intercalation of primary amines	*In situ* observation and analysis of vertical analyte diffusion
$H_{1-x}TBA_xCa_2Nb_3O_{10}$ (ref. 57)	Thin film	Stimuli responsive, UV-light decomposition of interlayer species	Vapor sensing, patterning film in microscale structures
TiO_2/SiO_2 with defect $H_3Sb_3P_2O_{14}$ containing a dye layer (ref. 84)	Defect 1D PC	Control of the "photonic window" by swelling of the defect layer	Fluorescent humidity sensor (switch on and off)
LTS/TiO_2 (ref. 55)	1D PC	Ultrahigh refractive index layer, stimuli responsive, swelling	Humidity sensing transparency switching
LTS/SiO_2 (ref. 55)			
LTS/$H_3Sb_3P_2O_{14}$ (ref. 55)	1D PC	Stimuli responsive, swelling	Humidity sensing, transparency switching
Graphene (ref. 67)	Thin film	Stimuli responsive, sensitive to strain	Tensile strain sensor
Graphene oxide (GO) (ref. 58)	Thin film	Stimuli responsive, swelling	Humidity sensor
Graphene oxide (GO) (ref. 68)	Thin film	Stimuli responsive, swelling	Vapor sensor, primarily for ethanol
GO/TiO_2 (ref. 85)	1D PC	Optical contrast/unspecified	DMSO liquid sensor and alkali pH sensor (both irreversible)
GO/TiO_2/(PEG-cross-linked PMVE-*co*-MA) (ref. 86)	1D PC	Optical contrast/unspecified	DMSO liquid sensor and alkali pH sensor (reversible)
GO/TiO_2 with PANI defect functionalized with Congo red (ref. 87)	Defect 1D PC	Non-responsive	Beta-glucan detection in liquids
GO hydrogel/TiO_2 with PANI defect functionalized with Congo red (ref. 87)	Defect 1D PC	Stimuli responsive, swelling, refractive index change	Beta-glucan detection in liquids

[a] MMO mixed metal oxide.

In terms of functionality, stimuli responsive sensors based on 2D materials can be grouped into different categories depending on the stimuli they can detect, *e.g.* vapor, liquid, temperature, and mechanically or magnetically responsive sensors.[7,10] In the following, we will highlight the different types of photonic sensors based on 2D materials, putting special emphasis on humidity, ion and vapor sensors, as these are currently the most investigated ones.

Table 2 Overview of the refractive index range of selected 2D materials at 633 nm. Note that the effective refractive indices are dependent on the relative humidity level

2D material	Refractive index @ 633 nm
LAPONITE®	1.47–1.51 (ref. 50)
LTS	1.75–2.50 (ref. 55)
$H_3Sb_3P_2O_{14}$	1.52–1.56 (ref. 41 and 55)
$HSbP_2O_8$	1.50–1.57 (ref. 72)
$H_{1-x}TBA_xTaP_2O_8$	1.38–1.55 (ref. 56)
$H_{3-x}TBA_xSb_3P_2O_{14}$	1.37–1.53 (ref. 56)
Mg–Al–NO_3 LDH	1.53 (ref. 59)
$H_{0.52-x}TMA_xTi_{0.87}O_2$	2 (@ 600 nm) (ref. 65)
Graphene	2–2.65 (ref. 67)

One of the very few examples of a colorimetric mechanical sensor (Fig. 4a)[67] based on 2D materials is derived from multilayer graphene nanoplatelets coated on a glass fibre. Under tensile strain or compressive stress, the thickness of the graphene layer decreases, resulting in a blue shift of the interference-based color (see eqn (1)).[67]

Photonic temperature sensors based on 2D materials include liquid crystalline $H_{0.52-x}TMA_xTi_{0.87}O_2$ and 1D PC Mg–Al–NO_3 LDH/TiO_2 sensors (Fig. 4b and c).[59,65] For these systems, the mechanisms behind the color changes are different. The Mg–Al–NO_3 LDH/TiO_2 1D PC relies on a conversion of the LDH to a mixed metal oxide (MMO) upon calcination.[59] Due to the structural change of the LDH to MMO, the RI decreases from 1.5 to 1.2, leading to a blue shift in the displayed color. However, the reverse phase change from MMO back to LDH is not spontaneous and requires hydrothermal treatment. Instead, the gradual and reversible color change with increasing temperature in the $H_{0.52-x}TMA_xTi_{0.87}O_2$ (TMA: tetramethylammonium) liquid crystal is based on a gradual thermoresponsive ionic density change.[65] Increasing the temperature leads to dissociation of TMA from the nanosheet surface with concomitant protonation of the nanosheets. This triggers a decrease in the surface potential of the nanosheets which causes a decrease in the distance between the charged sheets, hence a blue shift is observed with increasing temperature. In addition, the color change is reversible and fast, *i.e.* completed within 200 ms.[65]

The $H_{0.52-x}TMA_xTi_{0.87}O_2$ liquid crystal, representing a special class of fluid photonic structures, can be applied to detect the direction of magnetic flux as well as pH changes (Fig. 4d and e).[65] The detection of the magnetic flux direction is based on the fact that the $H_{0.52-x}TMA_xTi_{0.87}O_2$ sheets orient themselves orthogonal to the magnetic flux. This unusual alignment has only been reported for this kind of nanosheet. When the magnetic flux direction is changed, the sheets also change their orientation, leading to a change in illumination angle θ (see eqn (1)) and, hence, a color shift. $H_{0.52-x}TMA_xTi_{0.87}O_2$ liquid crystals have further been utilized as pH sensors. The pH detection is based on the protonation of the oxoanionic groups of $H_{0.52-x}TMA_xTi_{0.87}O_2$ with decreasing pH value. This leads to a decrease in electrostatic repulsion between the sheets, resulting in a color change. Note that even a small change in pH of 0.1 causes significant color changes detectable with the naked eye.[65]

The most common transduction mechanism in 2D nanosheet-based photonic sensors relies on changes in the dimensionality of the active component.[40,41,50,58] Changes in thickness of the nanosheet layer causing the color change are either due to intercalation[41,50,58] or ion exchange reactions.[40,66,80] The observed changes are typically large as they are maximized due to the preferred alignment of the nanosheets parallel to the substrate. The most common stimulus that is sensed with such architectures is humidity.[41,50,55,56,58,71,72] The first example of reversible humidity sensing by a photonic architecture based on 2D materials dates back to the 1990s, where LAPONITE® thin films were assembled by the sequential deposition of nanosheets from colloidal suspensions.[50] This was followed later with graphene oxide thin films (Fig. 4f) prepared by dip-coating,[58] and by various 1D PCs including $H_3Sb_3P_2O_{14}/SiO_2$ (Fig. 4g),[41] $H_3Sb_3P_2O_{14}/TiO_2$,[41] $HSbP_2O_8/TiO_2$,[72] LTSLTS/TiO_2,[55] LTS/SiO_2[55] and silk/silk-TiO_x[71] 1D PCs prepared by spin-coating. Most of these architectures show extremely fast response times on the order of milliseconds to a few seconds and an ultrahigh sensitivity (defined as colorshift (nm)/% RH) to the humidity stimulus.[41,50,58,72] Interestingly, for some of the structures, *e.g.* $H_3Sb_3P_2O_{14}/SiO_2$ and LTS/SiO_2 1D PCs, the RI contrast is cancelled at high relative humidity,[41,55] and as a consequence, the photonic structure turns transparent. This transparency switching is due to RI matching upon water intercalation into the structure as the high-RI nanosheet layer swells upon water uptake (effective RI decreases) and the textural pores of the low-RI layer are filled with water (effective RI increases).[41,55] The combination of fast response times and giant color shift in response to humidity enables the touchless tracking of the motion of a finger across the surface of a 1D PC (Fig. 4h), based on the humid atmosphere surrounding a human finger.[41] Touchless tracking of finger motion may be interesting in both touch- and touchless user interfaces for input or as feedback mechanism.

While humidity sensors continue to be of utmost importance, sensors that are capable of detecting and differentiating between volatile organic compounds (VOCs) are likewise of immense practical interest due to their broad application range, *e.g.* in environmental monitoring and medical diagnostics.[10,25,87–94] Photonic structures based on unmodified 2D materials have shown some potential in the field of vapor differentiation, *i.e.* as photonic noses.[68,72] We were able to show that different polar protic vapors could be distinguished from non-polar vapors by recording the time dependent optical shift of a $HSbP_2O_8/TiO_2$ 1D PC.[72] Using this combined read-out of spectral shift and response time, even constitutional isomers among the polar and protic vapors could be differentiated (Fig. 5a). In fact, the observed degree of vapor differentiation with a single-element photonic nose is among the best reported so far. The main reason for this high selectivity is due to the acidic nature of the nanosheet layer, which is able to selectively interact with

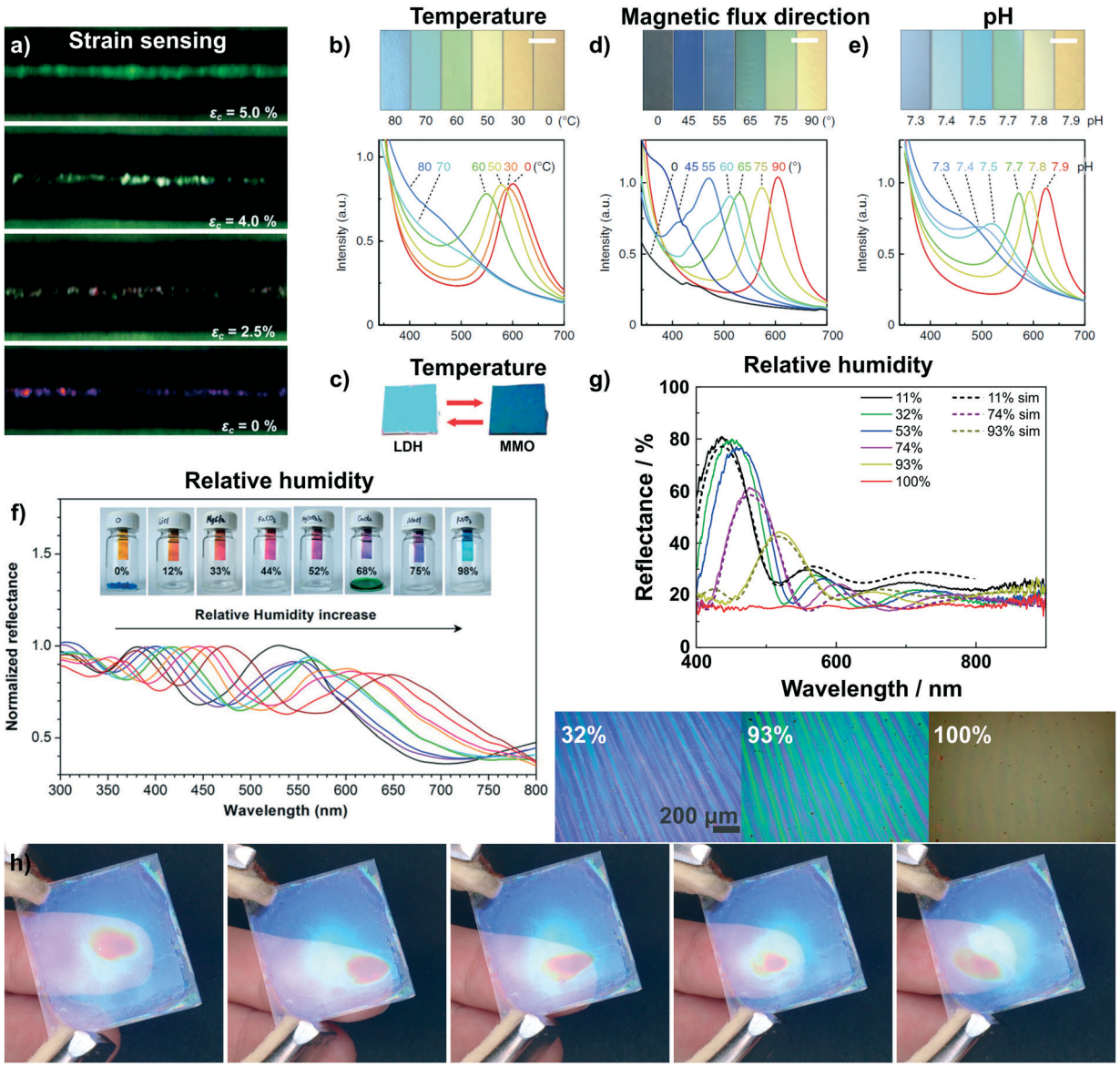

Fig. 4 Dynamic structural color changes in photonic architectures based on 2D materials, induced through various stimuli (see text). a) Variation in structural color of a graphene nanoplatelet interference sensor under different axial strain values;[67] b) sensing of temperature with a $H_{0.52-x}TMA_xTi_{0.87}O_2$ liquid crystal[65] and c) with Mg–Al–NO_3 LDH/TiO_2 1D PC.[59] d) Sensing of the magnetic flux direction[65] and e) pH with $H_{0.52-x}TMA_xTi_{0.87}O_2$ liquid crystals.[65] f) Humidity sensing with a graphene oxide thin film on a silicon substrate[59] and g) with a $H_3Sb_3P_2O_{14}/SiO_2$ 1D PC.[58] In g) also the reversible transparency switching is shown, which happens due to the cancellation of refractive index contrast upon water infiltration of the structure. In addition, due to their fast response time and high sensitivity to moisture the $H_3Sb_3P_2O_{14}/SiO_2$ 1D PC can be utilized to detect human finger motions in a touchless fashion, h).[41] Panel a) reprinted and adapted with permission from ref. 67, Copyright 2017 The Royal Society of Chemistry. Panel b), d) and e) reprinted and adapted with permission from ref. 65, Copyright 2016 Springer Nature. Panel c) reprinted and adapted with permission from ref. 59, Copyright 2012 The Royal Society of Chemistry. Panel f) reprinted with permission from ref. 58, Copyright 2015 American Chemical Society. Panel g) and h) reprinted and adapted with permission from ref. 41, Copyright 2015 John Wiley and Sons.

polar protic analytes through hydrogen bonding and acid–base interactions.[72] Graphene oxide thin films were also able to distinguish between polar protic vapors (see Fig. 5b).[68] For both graphene oxide thin films and $HSbP_2O_8/TiO_2$ 1D PC the sensing response is reversible.

Irreversible detection of analytes under certain conditions has also been used advantageously, especially for sensing trace amounts of analytes or to monitor analyte uptake processes in real-time. The latter is particularly intriguing as it allows for the label-free detection of otherwise optically silent processes.[40,80,82] 2D materials are ideally suited for such a detection scheme through intercalation and ion exchange. LAPONITE® thin films and LAPONITE®/TiO_2 1D PCs were utilized to differentiate between differently sized positively charged surfactants and between analytes with different functional groups by Lotsch and Ozin (Fig. 5c).[40]

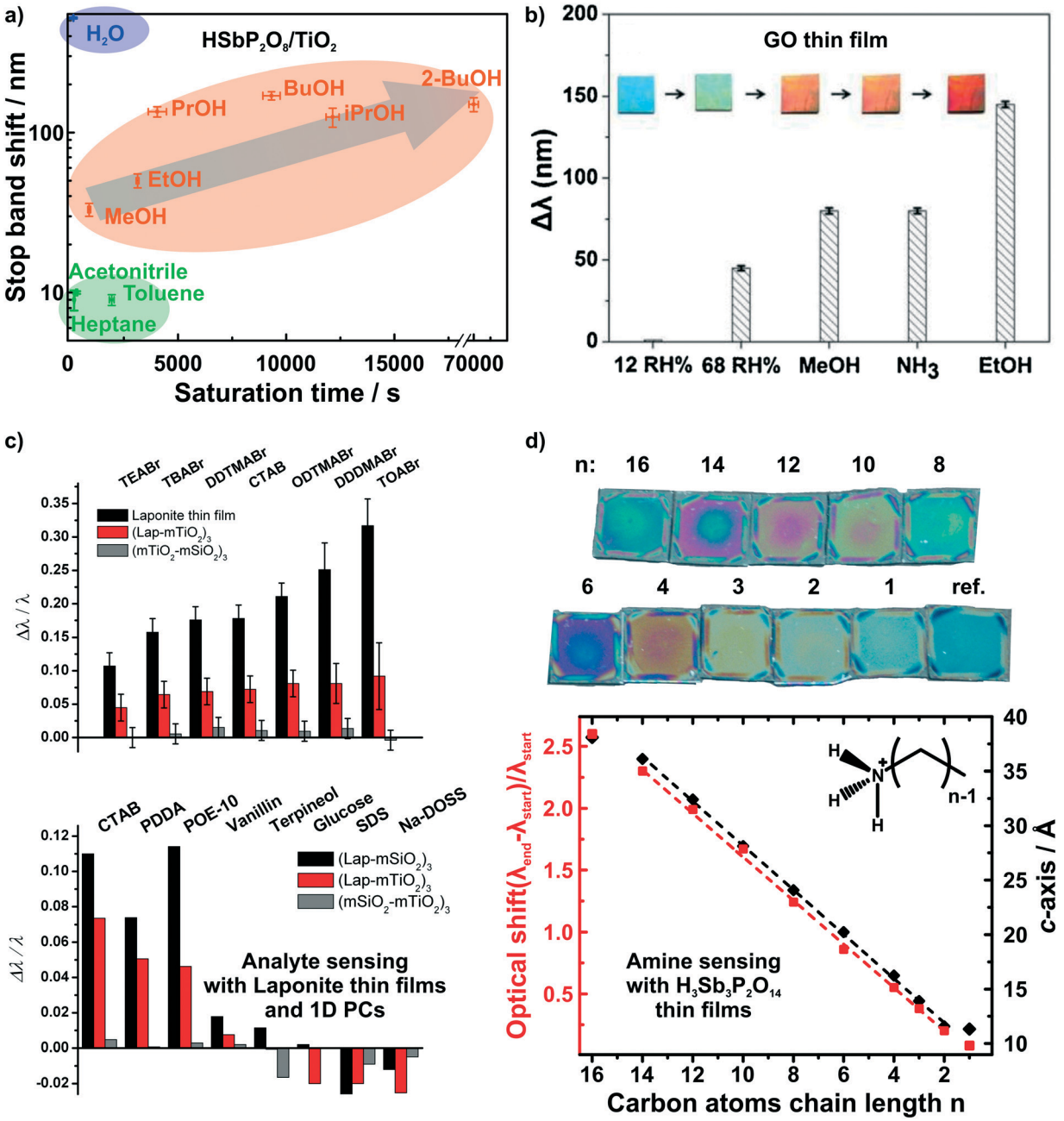

Fig. 5 Dynamic structural color changes caused by gaseous and liquid stimuli in 2D material based structures. Differentiation of polar and protic vapors with $HSbP_2O_8/TiO_2$ 1D PCs, a),[72] and graphene oxide thin films, b).[68] c) Identification of bulky ionic surfactants and molecules with different functional groups with LAPONITE® thin films and 1D PCs.[40] d) Primary alkylamine recognition with $H_3Sb_3P_2O_{14}$ thin films. The linear increase in the alkyl chain length results in linearly increasing *d*-spacing and hence, optical shift.[82] Panel a) reprinted with permission from ref. 72, Copyright 2016 John Wiley and Sons. Panel b) reprinted and adapted with permission from ref. 68, Copyright 2018 Elsevier. Panel c) reprinted and adapted with permission from ref. 40, Copyright 2008 John Wiley and Sons. Panel d) reprinted and adapted with permission from ref. 82, Copyright 2018 American Chemical Society.

Here, the dominant detection mechanism is based on ion exchange of the interlayer alkali cations by organic alkylammonium species.[40,80] Following the concomitant color shift, the uptake kinetics of the analytes were investigated and it was demonstrated that the initial state of the sensor could be recovered by the reverse ion exchange process.[40,80]

Recently, we were able to extend this theme to the intercalation of various primary and tertiary alkylamine vapors into $H_3Sb_3P_2O_{14}$ photonic thin films (Fig. 5d).[82] As the amines are protonated during intercalation, they are trapped in the interlayer space. Since the layer charge density of $H_3Sb_3P_2O_{14}$ is higher compared to LAPONITE® layers, we obtained a clearer correlation with the analyte size.[40,82] This is due to the fact

that the layer charge density governs the orientation and, hence, packing of the charged surfactant in the interlayer space. With increasing number of carbon atoms in the alkylchain we observed a linear increase in the intergallery spacing (*i.e.* *d*-values) and, as a consequence, in the optical shift for primary alkyl amines. Moreover, we could differentiate between similarly sized primary and tertiary alkylamines based on the intercalation time.[82] Intriguingly, by simulating the time-evolution of the optical spectra, we were able to monitor vertical diffusion of primary alkyamines into $H_3Sb_3P_2O_{14}/TiO_2$ 1D PCs in real time. In essence, this allows us study processes occurring at the molecular level like diffusion and layer expansion with a simple macroscopic optical read-out.[83] Therefore, optical architectures with 2D materials might help to add to the general understanding of diffusion phenomena and intercalation mechanisms of molecules in 2D materials.

Tuning dynamic color changes based on 2D materials

As both ion exchange and amine intercalation techniques in 2D materials as described above are irreversible under certain conditions, they can be used to permanently modify and fine-

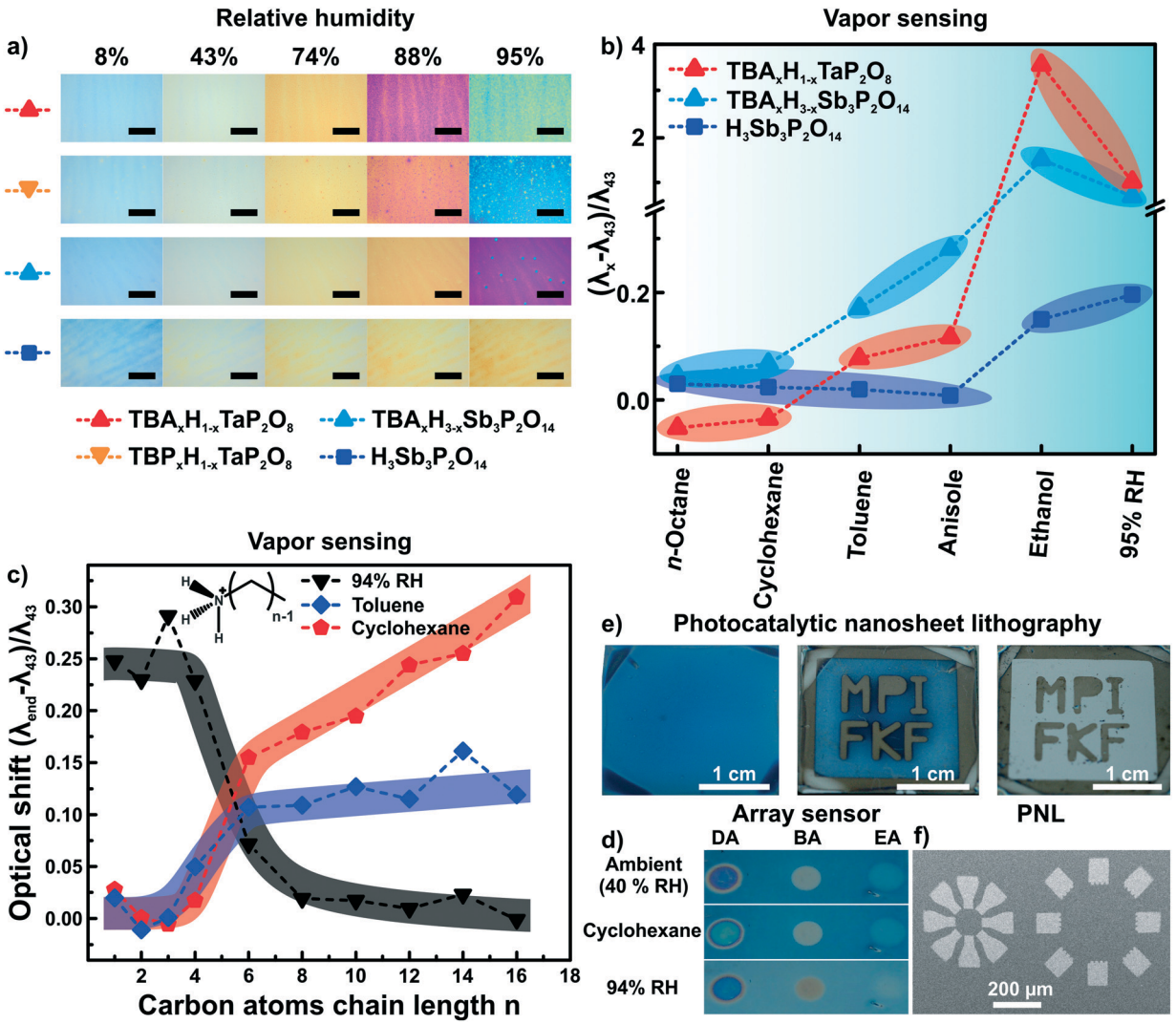

Fig. 6 Controlling the properties of nanosheet sensors by non-covalent functionalization. Effect of ion exchanging layered phosphate thin films with TBA on a) the sensitivity towards humidity, and b) the capability to distinguish between vapors with varying polarity.[56] c) Influence of primary alkylamine intercalation on the selectivity of $H_3Sb_3P_2O_{14}$ thin films.[82] d) Area resolved intercalation of primary alkylamines (DA decylamine, BA, butylamine and EA ethylamine) for creating a sensor array on a single $H_3Sb_3P_2O_{14}$ thin film and identification of vapor through characteristic color patterns with the functionalized thin films.[82] e) $H_{1-x}TBA_xCa_2Nb_3O_{10}$ area resolved control of the interlayer cation by photocatalytic decomposition of the interlayer species under UV-light with a mask. In the development step from the second to third picture the TBA containing areas get washed away.[57] f) Micron-scale structures obtained by this technique (photocatalytic nanosheet lithography), utilizing $H_{1-x}TBA_xCa_2Nb_3O_{10}$ as a negative photoresist.[57] Panel a) and b) reprinted and adapted with permission from ref. 56, Copyright 2017 John Wiley and Sons. Panel c) and d) reprinted and adapted with permission from ref. 82, Copyright 2018 American Chemical Society. Panel e) and f) reprinted and adapted with permission from ref. 57, Copyright 2017 John Wiley and Sons.

tune the sensor chemically. To highlight the effect of ion exchange on the vapor response characteristics, we studied the effect of exchanging the interlayer protons for TBA (tetrabutylammonium) on the vapor response characteristics.[56] The response of $H_{1-x}TBA_xTaP_2O_8$, $H_{3-x}TBA_xSb_3P_2O_{14}$ and $H_3Sb_3P_2O_{14}$ photonic thin films towards humidity and different organic vapors were recorded (Fig. 6a and b). The interlayer cation increased the sensitivity towards humidity in the high humidity regime (compare Fig. 6a, images 88% and 95% RH) and endowed the sensor with better performance in discriminating between and among non-polar and moderately polar vapors (Fig. 6b).[56] Comparable sensitivity and selectivity was observed for $H_{1-x}TBA_xCa_2Nb_3O_{10}$ photonic thin films.[57] Besides enhancing the sensitivity towards humidity, TBA modification allowed for fast (ms) tracking of polar and protic vapors.[56] All of these changes can be attributed to the role of the interlayer cation that acts as the gatekeeper by controlling the chemical nature as well as width of the interlayer space.[56,57]

At the same time, the vapor-phase amine intercalation into $H_3Sb_3P_2O_{14}$ thin films is a versatile chemical tool to fine tune the sensor's selectivity over an even large polarity range (Fig. 6c).[82] The vapor intercalation strategy is highly beneficial because it is a post-assembly modification approach requiring no optimization of the spin-coating procedure, which hence is generic for all subsequent amine modifications.[82,95] Due to the intercalation of amines with long alkyl chain lengths, considerably large responses for non-polar vapors were obtained for photonic structures based on 2D materials for the first time. Another attractive feature of the amine intercalation method is its local resolution. Hence, area resolved intercalation using a mask allows for the straightforward construction of an array sensor, which was used to distinguish between various vapors by the naked eye (Fig. 6d).[82]

We also utilized the concept of area resolved control of the interlayer species in $H_{1-x}TBA_xCa_2Nb_3O_{10}$ photonic thin films.[57] However, here the control was achieved by inducing locally resolved photocatalytic decomposition of the interlayer species TBA by the photocatalytically active host layer (*i.e.* $Ca_2Nb_3O_{10}^-$ nanosheets) under UV illumination (Fig. 6e). Therefore, the $H_{1-x}TBA_xCa_2Nb_3O_{10}$ photonic thin films can be used as a single UV-test strip with the areas exposed to UV-light getting thinner due to the decomposition of the interlayer species. Moreover, as the interlayer cation dictates the swelling properties of the photonic nanosheet thin films, the TBA containing areas were selectively etched away leaving behind the photocatalytically modified $H_{1-x}(NH_4)_xCa_2Nb_3O_{10}$ areas. Structures with lateral features of sizes smaller than 100 μm could be produced by this technique, termed photocatalytic nanosheet lithography (PNL). It is important to note that reproducibly achieving small lateral feature sizes with nanosheets is still difficult at the current stage. Research carried out with photonic structures based on modified 2D materials can therefore be useful also beyond sensing.[57]

Intercalation and ion exchange are both effective methods to tailor the functions of structures assembled from 2D materials.[56,82] However, other possibilities of tuning the photonic response of such structures exist, such as realizing different compositional structures[55] or changes in the design of the architectures leading to altered functions (Fig. 7).[66,80,84,87] Recent approaches include the fabrication of 1D PCs based on two different swellable 2D materials ("all-nanosheet Bragg stacks", Fig. 7a) and the creation of hybrid 1D PCs with organic polymers.[55,86,87] An alternative way to modify the optical response is by altering the porosity of the nanosheet layer through templating (Fig. 7b).[66,80] By carefully controlling the assembly conditions, this can lead to 1D PCs made out of the same materials having different porosities and, hence, effective RIs. Besides 1D PCs, also inverse opal-type 3D PC architectures have been realized with LAPONITE® nanosheets.[66]

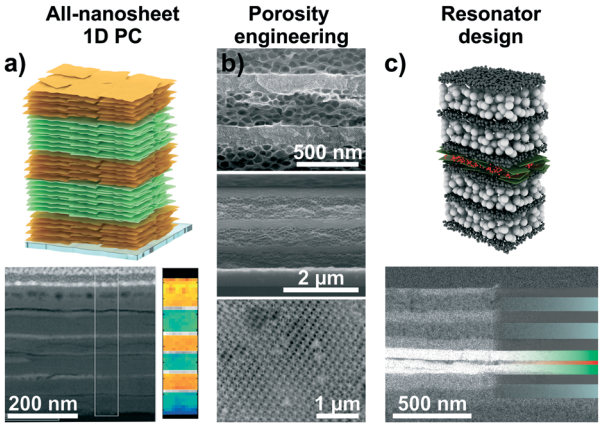

Fig. 7 Tailoring the functions of 2D material based photonic architectures by changing the composition and modifying the photonic lattice. a) 1D PCs based on LTS/$H_3Sb_3P_2O_{14}$ nanosheets with a schematic and a cross-section image including an EELS map.[55] b) Changing the porosity of 2D materials by templating with organic spheres. SEM cross-section images of different examples: top, LAPONITE®/TiO_2 1D PC, middle, all-LAPONITE® 1D PC based on different porosities,[80] and bottom, LAPONITE® 3D PC.[66] c) Utilizing nanosheet layers as defect layers in resonator structures: In the displayed case a TiO_2/SiO_2 1D PC with a $H_3Sb_3P_2O_{14}$ defect (green) containing a dye layer (red) was utilized to construct fluorescence turn-on and -off humidity sensors.[84] Panel a) reprinted and adapted with permission from ref. 55, Copyright 2018 John Wiley and Sons. Panel b) reprinted and adapted with permission from ref. 66 and 80, Copyright 2008 American Chemical Society. Panel c) reprinted and adapted with permission from ref. 84, Copyright 2017 John Wiley and Sons.

Another possibility is the design of photonic defect architectures based on 2D materials (Fig. 7c).[84,87] Such cavity-type structures with purposefully designed electrical field distributions across the multilayer can be used to create sensors with higher resolution or alternative read-out schemes. For example, a defect layer in a 1D PCs located in the middle of the stack induces creates optical states in the band gap, leading to a dip in the reflectance spectrum. As the narrow dip position can be read out with a higher precision compared to the broad reflectance maximum, this can lead to enhanced analyte resolution.[27,80] Alternatively, placing polymer spheres loaded with fluorescent molecules in the defect layer was used to design fluorescence turn-on and turn-off sensors. Here, the

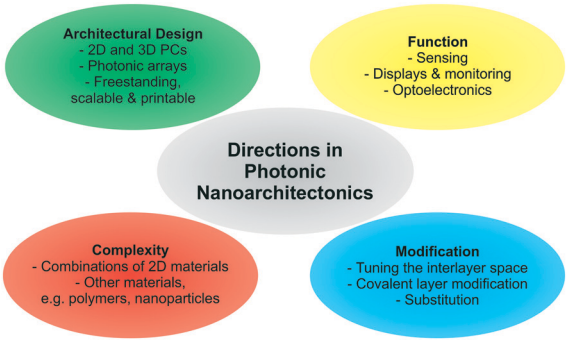

Fig. 8 Overview of future directions in photonic nanoarchitectonics based on stimuli-responsive 2D materials.

operating mode depends on the relative spectral positions of the humidity-tunable stopband and the fluorescence maximum, respectively. An example for the design of a photonic cavity structure based on 2D materials is shown in Fig. 7c.[84]

A bright future for 2D materials

As illustrated based on the above examples, a fine selection of inorganic 2D materials has already been used as the source of tunable structural color, with many more to come.

And yet, there is plenty of room left for innovation as the field matures. In the final section, some promising future directions will be highlighted (Fig. 8).

Although several 2D materials have been integrated into architectures for structural coloration, a plethora of new and existing 2D materials with stimuli-responsive properties are at hand, including for example layered Zintl phases, MXenes and Xenes, metal halogenides, and transition metal (di)chalcogenides.[42,44,49,76,77] Introducing these families of compounds with widely differing properties can result in novel functionalities. Moreover, combining different 2D materials with each other, with functional nanoparticles or with polymers in complex photonic architectures is still in its infancy and will unleash complex and enhanced functionality.

Besides cation exchange and spontaneous intercalation, smart strategies are needed to customize the sensor response by individually fine tuning the composition of the layers and the interlayer space. Besides cation exchange or intercalation,[56,82] anion exchange properties (*e.g.* in LDHs) can be used to detect anionic analytes. Moreover, the layer charge density of charged nanosheets can be adjusted to achieve different orientations of the interlayer species, thereby gradually fine tuning the interlayer spacing. In addition, intercalation by electrochemical methods are promising. Here, one can tailor the *d*-spacing, *e.g.* redox intercalation of Li[96–98] or bulky ammonium ions,[99] induce phase transitions (*e.g.* 2H → 1T MoS_2) and, hence, dynamically change the structural colors over a large range, which might be suitable for display technologies.[100,101]

A large and essentially unexplored area is the integration of covalently modified nanosheets into photonic architectures. Pre- or post-assembly covalent modification of the nanosheet layers through grafting is an excellent tool to endow them with analyte specific functionality. There are now many reports available describing how to tailor the properties of the nanosheets and parent layered materials by covalent modifications.[48,49,89,90,102–106] The reactions are as diverse as the different nanosheet compositions and structures and comprise reactions with thiols, including click reactions, electrophiles, such as alkyl iodides and diazonium salts, isocyanates, epoxides and coordination with metal salts.

Furthermore, with the recent focus on improving existing strategies and inventing new ones for quantitative nanosheet exfoliation, processing, and assembly, it is likely that scalable, as well as more complex photonic architectures based on 2D materials become readily available, like for example printable nanostructures and systems amenable to roll-to-roll processes.[51–54,107,108] This development will also enable the fabrication of more complex 2D and 3D photonic architectures based on 2D materials and the fabrication of freestanding photonic architectures based on 2D materials.[109]

In summary, this review highlights a new area in which 2D materials have the potential to excel, but unlike other directions, the use of 2D materials as building blocks for photonic architectures is still in its infancy. We have highlighted the diversity in composition and structures of the 2D materials used for structural coloration, and summarized the dynamic sensing response of 2D materials to various stimuli, which enables the tracking of otherwise optically silent processes. We discussed different strategies to tailor the functionality of photonic architectures based on 2D materials on the atomic scale by ion exchange and intercalation, as well as by changing the composition and design of the photonic architectures. To conclude, the future for creating tunable structural colors based on 2D materials is bright.

Conflicts of interest

There are no conflicts to declare.

Acknowledgements

Open Access funding provided by the Max Planck Society. Financial support was granted by the Max Planck Society, the University of Munich (LMU), the Center for NanoScience (CeNS), and the Deutsche Forschungsgemeinschaft (DFG) through the Cluster of Excellence Nanosystems Initiative Munich (NIM).

Notes and references

1 B. A. Bober, J. K. Ogata, V. E. Martinez, J. J. Hallinan, T. A. Leach and B. Negru, *J. Chem. Educ.*, 2018, **95**, 1004–1011.
2 H. Seo and S. Lee, *Sci. Rep.*, 2017, **7**, 44927.
3 Y. D. Afanasyev, G. T. Andrews and C. G. Deacon, *Am. J. Phys.*, 2011, **79**, 1079–1082.
4 R. A. Potyrailo, H. Ghiradella, A. Vertiatchikh, K. Dovidenko, J. R. Cournoyer and E. Olson, *Nat. Photonics*, 2007, **1**, 123.

5 E. Yablonovitch, *Phys. Rev. Lett.*, 1987, **58**, 2059–2062.
6 S. John, *Phys. Rev. Lett.*, 1987, **58**, 2486–2489.
7 G. Isapour and M. Lattuada, *Adv. Mater.*, 2018, **30**, 1707069.
8 G. von Freymann, V. Kitaev, B. V. Lotsch and G. A. Ozin, *Chem. Soc. Rev.*, 2013, **42**, 2528–2554.
9 L. D. Bonifacio, B. V. Lotsch, D. P. Puzzo, F. Scotognella and G. A. Ozin, *Adv. Mater.*, 2009, **21**, 1641–1646.
10 C. Fenzl, T. Hirsch and O. S. Wolfbeis, *Angew. Chem., Int. Ed.*, 2014, **53**, 3318–3335.
11 P. Lova, G. Manfredi and D. Comoretto, *Adv. Opt. Mater.*, 2018, **0**, 1800730.
12 M. E. Calvo, S. Colodrero, N. Hidalgo, G. Lozano, C. Lopez-Lopez, O. Sanchez-Sobrado and H. Miguez, *Energy Environ. Sci.*, 2011, **4**, 4800–4812.
13 H. Shen, Z. Wang, Y. Wu and B. Yang, *RSC Adv.*, 2016, **6**, 4505–4520.
14 J. Ge and Y. Yin, *Angew. Chem., Int. Ed.*, 2011, **50**, 1492–1522.
15 Y. Zhao, Z. Xie, H. Gu, C. Zhu and Z. Gu, *Chem. Soc. Rev.*, 2012, **41**, 3297–3317.
16 K. Ariga and M. Ebara, *Materials Nanoarchitectonics*, Wiley-VCH, Weinheim, 2018.
17 K. Ariga, Q. Ji, J. P. Hill, Y. Bando and M. Aono, *NPG Asia Mater.*, 2012, **4**, e17.
18 Y. J. Li, Y. Yan, Y. S. Zhao and J. Yao, *Adv. Mater.*, 2016, **28**, 1319–1326.
19 Y. Yan, J. Ye, K. Wang, J. Yao and Y. S. Zhao, *Small*, 2016, **14**, 1702698.
20 O. Stenzel, in *The Physics of Thin Film Optical Spectra: An Introduction*, Springer International Publishing, Cham, 2016, pp. 131–161, DOI: 10.1007/978-3-319-21602-7_7.
21 K. Szendrei-Temesi, *PhD thesis*, University of Munich, 2018.
22 T. Gao, J. Gao and M. J. Sailor, *Langmuir*, 2002, **18**, 9953–9957.
23 J. Gao, T. Gao, Y. Y. Li and M. J. Sailor, *Langmuir*, 2002, **18**, 2229–2233.
24 G. Lu and J. T. Hupp, *J. Am. Chem. Soc.*, 2010, **132**, 7832–7833.
25 H. Xu, P. Wu, C. Zhu, A. Elbaz and Z. Z. Gu, *J. Mater. Chem. C*, 2013, **1**, 6087–6098.
26 S. Y. Choi, M. Mamak, G. von Freymann, N. Chopra and G. A. Ozin, *Nano Lett.*, 2006, **6**, 2456–2461.
27 M. C. Fuertes, F. J. López-Alcaraz, M. C. Marchi, H. E. Troiani, V. Luca, H. Míguez and G. J. A. A. Soler-Illia, *Adv. Funct. Mater.*, 2007, **17**, 1247–1254.
28 M. E. Calvo, O. Sánchez-Sobrado, S. Colodrero and H. Míguez, *Langmuir*, 2009, **25**, 2443–2448.
29 Z. Wu, D. Lee, M. F. Rubner and R. E. Cohen, *Small*, 2007, **3**, 1445–1451.
30 L. D. Bonifacio, D. P. Puzzo, S. Breslav, B. M. Willey, A. McGeer and G. A. Ozin, *Adv. Mater.*, 2010, **22**, 1351–1354.
31 L. D. Bonifacio, G. A. Ozin and A. C. Arsenault, *Small*, 2011, **7**, 3153–3157.
32 F. M. Hinterholzinger, A. Ranft, J. M. Feckl, B. Rühle, T. Bein and B. V. Lotsch, *J. Mater. Chem.*, 2012, **22**, 10356–10362.
33 A. Ranft, F. Niekiel, I. Pavlichenko, N. Stock and B. V. Lotsch, *Chem. Mater.*, 2015, **27**, 1961–1970.
34 B. V. Lotsch, F. Scotognella, K. Moeller, T. Bein and G. A. Ozin, *Proc. SPIE*, 2010, **7713**, DOI: 10.1117/12.854703.
35 Y. Kang, J. J. Walish, T. Gorishnyy and E. L. Thomas, *Nat. Mater.*, 2007, **6**, 957.
36 Z. Wang, J. Zhang, J. Xie, C. Li, Y. Li, S. Liang, Z. Tian, T. Wang, H. Zhang, H. Li, W. Xu and B. Yang, *Adv. Funct. Mater.*, 2010, **20**, 3784–3790.
37 Z. Wang, J. Zhang, J. Li, J. Xie, Y. Li, S. Liang, Z. Tian, C. Li, Z. Wang, T. Wang, H. Zhang and B. Yang, *J. Mater. Chem.*, 2011, **21**, 1264–1270.
38 Z. Wang, J. Zhang, Z. Wang, H. Shen, J. Xie, Y. Li, L. Lin and B. Yang, *J. Mater. Chem. C*, 2013, **1**, 977–983.
39 P. Lova, G. Manfredi, L. Boarino, A. Comite, M. Laus, M. Patrini, F. Marabelli, C. Soci and D. Comoretto, *ACS Photonics*, 2015, **2**, 537–543.
40 B. V. Lotsch and G. A. Ozin, *Adv. Mater.*, 2008, **20**, 4079–4084.
41 K. Szendrei, P. Ganter, O. Sànchez-Sobrado, R. Eger, A. Kuhn and B. V. Lotsch, *Adv. Mater.*, 2015, **27**, 6341–6348.
42 R. Ma and T. Sasaki, *Adv. Mater.*, 2010, **22**, 5082–5104.
43 R. Ma and T. Sasaki, *Acc. Chem. Res.*, 2015, **48**, 136–143.
44 V. Nicolosi, M. Chhowalla, M. G. Kanatzidis, M. S. Strano and J. N. Coleman, *Science*, 2013, **340**, 1226419.
45 S. Z. Butler, S. M. Hollen, L. Cao, Y. Cui, J. A. Gupta, H. R. Gutierrez, T. F. Heinz, S. S. Hong, J. Huang, A. F. Ismach, E. Johnston-Halperin, M. Kuno, V. V. Plashnitsa, R. D. Robinson, R. S. Ruoff, S. Salahuddin, J. Shan, L. Shi, M. G. Spencer, M. Terrones, W. Windl and J. E. Goldberger, *ACS Nano*, 2013, **7**, 2898–2926.
46 F. Geng, R. Ma, Y. Ebina, Y. Yamauchi, N. Miyamoto and T. Sasaki, *J. Am. Chem. Soc.*, 2014, **136**, 5491–5500.
47 J. Wan, S. D. Lacey, J. Dai, W. Bao, M. S. Fuhrer and L. Hu, *Chem. Soc. Rev.*, 2016, **45**, 6742–6765.
48 S. Bertolazzi, M. Gobbi, Y. Zhao, C. Backes and P. Samorì, *Chem. Soc. Rev.*, 2018, **47**, 6845–6888.
49 S. Jiang, M. Q. Arguilla, N. D. Cultrara and J. E. Goldberger, *Acc. Chem. Res.*, 2015, **48**, 144–151.
50 E. R. Kleinfeld and G. S. Ferguson, *Chem. Mater.*, 1995, **7**, 2327–2331.
51 F. Bonaccorso, A. Bartolotta, J. N. Coleman and C. Backes, *Adv. Mater.*, 2016, **28**, 6136–6166.
52 K. Matsuba, C. Wang, K. Saruwatari, Y. Uesusuki, K. Akatsuka, M. Osada, Y. Ebina, R. Ma and T. Sasaki, *Sci. Adv.*, 2017, **3**, e1700414.
53 J. Kang, V. K. Sangwan, J. D. Wood and M. C. Hersam, *Acc. Chem. Res.*, 2017, **50**, 943–951.
54 J. Zhu and M. C. Hersam, *Adv. Mater.*, 2017, **29**, 1603895.
55 K. Szendrei-Temesi, O. Sanchez-Sobrado, S. B. Betzler, K. M. Durner, T. Holzmann and B. V. Lotsch, *Adv. Funct. Mater.*, 2018, **28**, 1705740.
56 P. Ganter, L. M. Schoop and B. V. Lotsch, *Adv. Mater.*, 2017, **29**, 1604884.
57 P. Ganter and B. V. Lotsch, *Angew. Chem., Int. Ed.*, 2017, **56**, 8389–8392.

58 H. Chi, Y. J. Liu, F. Wang and C. He, *ACS Appl. Mater. Interfaces*, 2015, **7**, 19882–19886.
59 J. Han, Y. Dou, M. Wei, D. G. Evans and X. Duan, *RSC Adv.*, 2012, **2**, 10488–10491.
60 C. Backes, T. M. Higgins, A. Kelly, C. Boland, A. Harvey, D. Hanlon and J. N. Coleman, *Chem. Mater.*, 2017, **29**, 243–255.
61 K. R. Paton, E. Varrla, C. Backes, R. J. Smith, U. Khan, A. O'Neill, C. Boland, M. Lotya, O. M. Istrate, P. King, T. Higgins, S. Barwich, P. May, P. Puczkarski, I. Ahmed, M. Moebius, H. Pettersson, E. Long, J. Coelho, S. E. O'Brien, E. K. McGuire, B. M. Sanchez, G. S. Duesberg, N. McEvoy, T. J. Pennycook, C. Downing, A. Crossley, V. Nicolosi and J. N. Coleman, *Nat. Mater.*, 2014, **13**, 624–630.
62 J. N. Coleman, M. Lotya, A. O'Neill, S. D. Bergin, P. J. King, U. Khan, K. Young, A. Gaucher, S. De, R. J. Smith, I. V. Shvets, S. K. Arora, G. Stanton, H.-Y. Kim, K. Lee, G. T. Kim, G. S. Duesberg, T. Hallam, J. J. Boland, J. J. Wang, J. F. Donegan, J. C. Grunlan, G. Moriarty, A. Shmeliov, R. J. Nicholls, J. M. Perkins, E. M. Grieveson, K. Theuwissen, D. W. McComb, P. D. Nellist and V. Nicolosi, *Science*, 2011, **331**, 568–571.
63 S. Manzeli, D. Ovchinnikov, D. Pasquier, O. V. Yazyev and A. Kis, *Nat. Rev. Mater.*, 2017, **2**, 17033.
64 J.-C. P. Gabriel, F. Camerel, B. J. Lemalre, H. Desvaux, P. Davidson and P. Batail, *Nature*, 2001, **413**, 504–508.
65 K. Sano, Y. S. Kim, Y. Ishida, Y. Ebina, T. Sasaki, T. Hikima and T. Aida, *Nat. Commun.*, 2016, **7**, 12559.
66 B. V. Lotsch and G. A. Ozin, *J. Am. Chem. Soc.*, 2008, **130**, 15252–15253.
67 Y. Deng, S. Gao, J. Liu, U. Gohs, E. Mäder and G. Heinrich, *Mater. Horiz.*, 2017, **4**, 389–395.
68 T. Gong, X. Zhang, Y. Fu, G. Zhou, H. Chi and T. Li, *Sens. Actuators, B*, 2018, **261**, 83–90.
69 S. Colodrero, M. Ocaña and H. Míguez, *Langmuir*, 2008, **24**, 4430–4434.
70 M. C. Fuertes, S. Colodrero, G. Lozano, A. R. González-Elipe, D. Grosso, C. Boissière, C. Sánchez, G. J. D. A. A. Soler-Illia and H. Míguez, *J. Phys. Chem. C*, 2008, **112**, 3157–3163.
71 E. Colusso, G. Perotto, Y. Wang, M. Sturaro, F. Omenetto and A. Martucci, *J. Mater. Chem. C*, 2017, **5**, 3924–3931.
72 P. Ganter, K. Szendrei and B. V. Lotsch, *Adv. Mater.*, 2016, **28**, 7436–7442.
73 A. Molle, J. Goldberger, M. Houssa, Y. Xu, S.-C. Zhang and D. Akinwande, *Nat. Mater.*, 2017, **16**, 163–169.
74 M. Q. Arguilla, J. Katoch, K. Krymowski, N. D. Cultrara, J. Xu, X. Xi, A. Hanks, S. Jiang, R. D. Ross, R. J. Koch, S. Ulstrup, A. Bostwick, C. Jozwiak, D. W. McComb, E. Rotenberg, J. Shan, W. Windl, R. K. Kawakami and J. E. Goldberger, *ACS Nano*, 2016, **10**, 9500–9508.
75 M. Q. Arguilla, N. D. Cultrara, Z. J. Baum, S. Jiang, R. D. Ross and J. E. Goldberger, *Inorg. Chem. Front.*, 2017, **4**, 378–386.
76 B. Anasori, M. R. Lukatskaya and Y. Gogotsi, *Nat. Rev. Mater.*, 2017, **2**, 16098.
77 M. Chhowalla, H. S. Shin, G. Eda, L.-J. Li, K. P. Loh and H. Zhang, *Nat. Chem.*, 2013, **5**, 263–275.
78 D. Weber, L. M. Schoop, V. Duppel, J. M. Lippmann, J. Nuss and B. V. Lotsch, *Nano Lett.*, 2016, **16**, 3578–3584.
79 Y. Dou, J. Han, T. Wang, M. Wei, D. G. Evans and X. Duan, *J. Mater. Chem.*, 2012, **22**, 14001–14007.
80 B. V. Lotsch and G. A. Ozin, *ACS Nano*, 2008, **2**, 2065–2074.
81 M. Osada and T. Sasaki, *Adv. Mater.*, 2012, **24**, 210–228.
82 P. Ganter, L. M. Schoop, M. Däntl and B. V. Lotsch, *Chem. Mater.*, 2018, **30**, 2557–2565.
83 K. Szendrei-Temesi, A. Jiménez-Solano and B. V. Lotsch, *Adv. Mater.*, 2018, **30**, 1803730.
84 K. Szendrei, A. Jiménez-Solano, G. Lozano, B. V. Lotsch and H. Míguez, *Adv. Opt. Mater.*, 2017, **5**, 1700663.
85 C. Yao, J. Zhao, H. Ge, J. Ren, T. Yin, Y. Zhu and L. Ge, *Colloids Surf., A*, 2014, **452**, 89–94.
86 C. Yao, J. Ren, C. Liu, T. Yin, Y. Zhu and L. Ge, *ACS Appl. Mater. Interfaces*, 2014, **6**, 16727–16733.
87 J. Ren, H. Xuan, C. Liu, C. Yao, Y. Zhu, X. Liu and L. Ge, *RSC Adv.*, 2015, **5**, 77211–77216.
88 X. Liu, T. Ma, N. Pinna and J. Zhang, *Adv. Funct. Mater.*, 2017, 1702168, DOI: 10.1002/adfm.201702168.
89 S. Presolski and M. Pumera, *Mater. Today*, 2016, **19**, 140–145.
90 X. Chen and A. R. McDonald, *Adv. Mater.*, 2016, **28**, 5738–5746.
91 W. Yang, L. Gan, H. Li and T. Zhai, *Inorg. Chem. Front.*, 2016, **3**, 433–451.
92 J. Zhang, X. Liu, G. Neri and N. Pinna, *Adv. Mater.*, 2016, **28**, 795–831.
93 S. Yang, C. Jiang and S.-H. Wei, *Appl. Phys. Rev.*, 2017, **4**, 021304.
94 P. K. Kannan, D. J. Late, H. Morgan and C. S. Rout, *Nanoscale*, 2015, **7**, 13293–13312.
95 A. von Mankowski, K. Szendrei-Temesi, C. Koschnick and B. V. Lotsch, *Nanoscale Horiz.*, 2018, **3**, 383–390.
96 A. M. Dimiev, G. Ceriotti, N. Behabtu, D. Zakhidov, M. Pasquali, R. Saito and J. M. Tour, *ACS Nano*, 2013, **7**, 2773–2780.
97 W. Bao, J. Wan, X. Han, X. Cai, H. Zhu, D. Kim, D. Ma, Y. Xu, J. N. Munday, H. D. Drew, M. S. Fuhrer and L. Hu, *Nat. Commun.*, 2014, **5**, 4224.
98 F. Xiong, H. Wang, X. Liu, J. Sun, M. Brongersma, E. Pop and Y. Cui, *Nano Lett.*, 2015, **15**, 6777–6784.
99 C. Wang, Q. He, U. Halim, Y. Liu, E. Zhu, Z. Lin, H. Xiao, X. Duan, Z. Feng, R. Cheng, N. O. Weiss, G. Ye, Y.-C. Huang, H. Wu, H.-C. Cheng, I. Shakir, L. Liao, X. Chen, W. A. Goddard Iii, Y. Huang and X. Duan, *Nature*, 2018, **555**, 231.
100 A. C. Arsenault, D. P. Puzzo, I. Manners and G. A. Ozin, *Nat. Photonics*, 2007, **1**, 468.
101 D. P. Puzzo, A. C. Arsenault, I. Manners and G. A. Ozin, *Angew. Chem., Int. Ed.*, 2009, **48**, 943–947.
102 S. Jiang, K. Krymowski, T. Asel, M. Q. Arguilla, N. D. Cultrara, E. Yanchenko, X. Yang, L. J. Brillson, W. Windl and J. E. Goldberger, *Chem. Mater.*, 2016, **28**, 8071–8077.

103 C. R. Ryder, J. D. Wood, S. A. Wells, Y. Yang, D. Jariwala, T. J. Marks, G. C. Schatz and M. C. Hersam, *Nat. Chem.*, 2016, **8**, 597–602.
104 D. Mochizuki, K. Kumagai, M. M. Maitani and Y. Wada, *Angew. Chem., Int. Ed.*, 2012, **51**, 5452–5455.
105 F. Kishimoto, T. Ano, D. Mochizuki, T. Terauchi, M. M. Maitani, E. Suzuki and Y. Wada, *RSC Adv.*, 2016, **6**, 73830–73841.
106 B. M. Mosby, A. Diaz and A. Clearfield, *Dalton Trans.*, 2014, **43**, 10328–10339.
107 D. McManus, S. Vranic, F. Withers, V. Sanchez-Romaguera, M. Macucci, H. Yang, R. Sorrentino, K. Parvez, S.-K. Son, G. Iannaccone, K. Kostarelos, G. Fiori and C. Casiraghi, *Nat. Nanotechnol.*, 2017, **12**, 343–350.
108 H.-L. Liang, M. M. Bay, R. Vadrucci, C. H. Barty-King, J. Peng, J. J. Baumberg, M. F. L. De Volder and S. Vignolini, *Nat. Commun.*, 2018, **9**, 4632.
109 M. E. Calvo, O. Sánchez Sobrado, G. Lozano and H. Míguez, *J. Mater. Chem.*, 2009, **19**, 3144–3148.